Penerbit Akademia Baru

Journal of Advanced Research in Fluid Mechanics and Thermal Sciences

Journal homepage: www.akademiabaru.com/arfmts.html
ISSN: 2289-7879

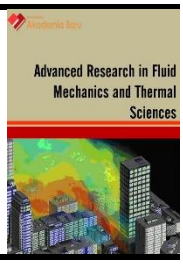

Experimental Investigation of Aerodynamic Performance of a Wind Turbine Blade Undergoing Pure Pitch and Plunge Motions

Open Access

Mohammad Hossein Razavi Dehkordi[1], Mohammad Reza Soltani[2,3,*], Ali Reza Davari[1]

[1] Aerospace division, Department of Engineering, Science and Research Branch, Islamic Azad University, Tehran, Iran
[2] Department of Aerospace Engineering, Sharif University of Technology, Tehran, Iran
[3] Presently visiting Professor, William E. Boeing Department of Aeronautics and Astronautics, University of Washington, Seattle, WA, USA

ARTICLE INFO

Article history:
Received 26 October 2019
Received in revised form 25 November 2019
Accepted 6 December 2019
Available online 15 March 2020

ABSTRACT

In this paper, extensive experimental tests were carried out for an aerodynamic characterization of the airfoil cross-section of a wind turbine blade. The wind turbine blade cross-sections are usually exposed to unsteady pitch and plunge oscillations. One way to increase the power of blade, is to improve it's aerodynamic performance, so it is necessary to study and compare the unsteady aerodynamic behavior of the airfoil. The aerodynamic behavior of turbine blades are dependent on several parameters including initial angle of attack, reduced frequency and oscillation amplitude. In this study, reduced frequency and oscillation amplitude assumed constant and the initial angle of attack of the model was varied in both pitch and plunge oscillations. Therefore, the aerodynamic behavior of the model was investigated under motions with similar conditions before, near and after of the static stall angles of attack. The vertical displacement of the plunge motion was selected such that the equivalent angle of attack in plunge motion is approximately equal to the oscillation amplitude in the pitch motion. All tests were conducted at a constant Reynolds number of 0.27×10^6. The practical results of this study indicate that the choice of a pitch or plunge motion, granted both are feasible, depends on the requirements and significance of aerodynamic forces and the decisive for ruling cannot be made about which motion guarantees the best aerodynamic performance at all angles of attack.

Keywords:
Pitch oscillation; plunge oscillation; reduced frequency; lift; moment; pressure distribution

1. Introduction

In recent years, unsteady flow physics and its application in scientific and industrial areas, such as renewable energies, wind turbines, and MAVs, have subjects of much debate. Despite the advancements in numerical methods, experimental studies still play a significant role in industrial developments and resolving the problems. Creating unsteady oscillations such as pitching or plunging motions in wind tunnels can help develop a better understanding of unsteady flows [1-8].

* *Corresponding author.*
E-mail address: msoltani@sharif.edu, reza2@uw.edu (Mohammad Reza Soltani)

Razavi Dehkordi *et al.,* determine the aerodynamic characteristics of an airfoil undergoing static, dynamic pitch, dynamic plunge and dynamic combined pitch and plunge motions for various cases. They are focus on the effects of reduced frequencies and mean angles of attack on the surface pressure distribution and on the corresponding lift of the airfoil oscillating in either pure pitch or in combined pitch-plunge motions. Results shown that Pitch oscillation seems to have dominant role in the pitch-plunge oscillation case [9].

Soltani *et al.,* performed experimental tests on the same airfoil undergoing plunge motion. Reduced frequency varied from 0.03 to 0.06, the amplitude of plunge ±0.15 m and the initial mean angles of attacks were set to 0°, 10° and 18°. The aerodynamic behaviour of the model and its dependency on the reduced frequency, angles of attack, etc. were similar to their previous pure pitching motion study, however, the magnitudes of the aerodynamic loads as well as the width of the hysteresis loops for the plunge case were different [10].

Dong-Ha Kim and his colleagues, investigated the aerodynamic behaviour of pitching airfoil at low Reynolds numbers, and fixed reduced frequency. Their results mentions that, through the flow visualization, the first and second vortices depends on Reynolds number. With the change in Reynolds number, the hysteresis lift and drag loops were change relatively [11].

The effect of blade pitch angle on vertical axis wind turbines on aerodynamic efficiency and power coefficient of these blades was investigated by Yonghui *et al.*, In this study, four quartiles were defined for the direction angle of a rotation period. Upwind, leeward, downwind and windward. The authors founded that, in all operational areas of a two-dimensional wind turbine blade, the appropriate pitch control angle, improves the blade efficiency and increases the turbine power coefficient than the fixed turbine blade [12].

Ansari *et al.*, studied the effect of using the different tip blade for determine the range of pitch angle and wind speed to improve the wind turbine performance. they showed that using tip plates for wind turbines performance improvement can only occur if the turbine blade pitch angle is set at the maximum output power based on the given wind speed [13].

Moriche *et al.,* studies have investigated the effects of changing the initial angle of attack of the pitch motion and the phase change between pitch and heaving motions on the aerodynamic forces. They founded that, in the aerodynamic forces, the viscous effects were negligible compared to the effects of apparent mass and circulation of flow. Their results, in comparison with previous studies, showed that significant progress in predicting mean thrust and smaller advancement in the lift coefficient prediction [14].

Tabrizian *et al.,* studied the surface pressure of a supercritical airfoil undergoing pure pitch, plunge and combined pitch-plunge motions at all ranges of angles of attack that involve before, near and after of static stall angle of attack. They fixed Reynolds number and reduced frequency and investigated the stability of airfoil at three different areas. In pure pitch, at the attached flow region the LEV grew and shrunk over the upper surface but in the light stall region the LEV spilled on the airfoil while a small partial LEV remained at the leading edge. In the deep stall region the LEV spilled entirely and the flow was fully separated. Forcing the airfoil to undergoing combined motion, improved the stability condition in all cases [15].

Gross was studied a wing section with a specific airfoil to investigate the effect of a harmonic heaving/plunging motion on the unsteady aerodynamics. Reduced frequency of motion varied from 0.35 to 1.4 and the Reynolds number fixed at 200000. At 10° mean angle of attack for the plunging motion, the good agreement between the unsteady lift and prediction of Theodorsen theory. With increasing the mean angle of attack up to 14°, the separated flow formed from the suction side of the wing. As the mean angle of attack increased to 16°, model is wholly stalled. However, when model

exposed to a low amplitude plunging motion, the flow reattached and the mean lift was increased [16].

In another research, Geng and Kalkman, reported the results of an extensive numerical simulation of the unsteady flow around a pitching NACA0012 airfoil at a constant Reynolds number of 1.35×10^5 at high angles of attack up to dynamic stall. They investigated influence of the large number of parameters on the numerical results. They compared their numerical results with the exciting experimental data. This comparison showed that an adequate agreement for the upstroke portion of the pitch motion, while for the downstroke portion of motion some differences appeared. These differences are investigated in more details by considering the results from a 2.5D Large Eddy Simulation (LES), which provides deep and complementary insights into the flow behaviour during dynamic stall at the selected Reynolds number [17].

Numerical studies on a special airfoil that Sinusoidal bumps height located at the leading edge of the airfoil, have been carried out by kunya *et al.,* Studies at the low Reynolds number and the angles of attack of the airfoil varied from -10 to 25 degrees. At different angles of attack, they investigated the effect of bumps on the lift coefficient and the effect of flow separation [18].

The effect of leading edge and trailing edge geometries, on the overall aerodynamic performance of a flat plate at various angles of attack and at different reduced frequencies, was investigated by Leknys and Arjomandi. They founded that, for all leading and trailing edge combinations, increasing the rotation rate increased the magnitude of the localized low pressure on the upper surface of the flat plate which resulted in the lift increasing. This study upholds that vortex lift is limited by the maximum angle of attack and rotation rate [19].

To the best knowledge of the authors, no experimental studies have been conducted so far to create identical oscillatory conditions for pitch and plunge motions and conduct pure pitch and plunge oscillations under similar conditions for comparison purposes. In this study, an airfoil was subjected to both pitch and plunge oscillatory motions that were created using proper equipment. An effort was made to compare aerodynamic coefficients corresponding to the pressure distribution over the upper and lower surfaces of the model under identical oscillation conditions—including the initial angle of attack, oscillation amplitude, and reduced frequency. In the end, the optimal oscillatory motion was recommended for different angles of attack in the case where both oscillations are feasible. Otherwise, combined pitch–plunge motions are alternatively employed for the experiment if none can individually fulfil the aerodynamic requirements.

2. Experimental Facility

All tests were performed in a low subsonic wind tunnel of an open suction circuit type with a dimensions of test-section of 2m×1m×0.8m. The speed of tunnel could be changed from 10 to 100 m/s. Experiments were conducted at a Reynolds Numbers variation between 0.13 to 1.3 million. For decreasing the turbulence level of flow, the three anti turbulence screens and a honeycomb were installed in the settling chamber. It could be concluded that due to the changing the atmospheric pressure, speed in the test-section might change lowly. To prevent the changes, the speed of tunnel was checked continuously.

A 2D section of a wind turbine blade model was applied in the tests which it's chord and span was 25cm and 80cm, respectively. The ports for measuring the pressure distribution over the airfoil surface dense around the leading edge on the upper and lower surfaces of the model (Figure 1).

The differential pressure transducers by ±1 psi ranges was applied to measure the surface pressure data. The data were processed by an analogue to digital board. A low pass filter was used to filter the digital data.

The oscillating mechanism consists of two servo motors, gearbox, etc. It has the ability to create pure pitch and plunge motions separately. Also, it can change the initial angle of attack, the amplitudes and the frequencies of pitch and plunge motions. The pitch and plunge motions are completely independent of each other. Moreover, all data acquisition and data reduction routines were developed from the scratch for these experiments. The model is pitched around its 0.25 chord point. Figure 2 shows the oscillation mechanism that designed and manufactured for the special experiment tests.

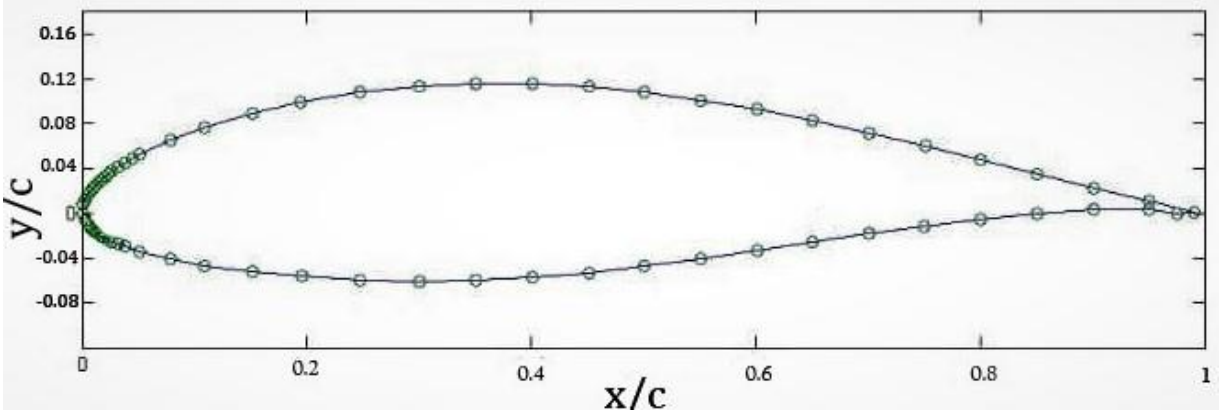

Fig. 1. Location of the pressure ports along the model surface

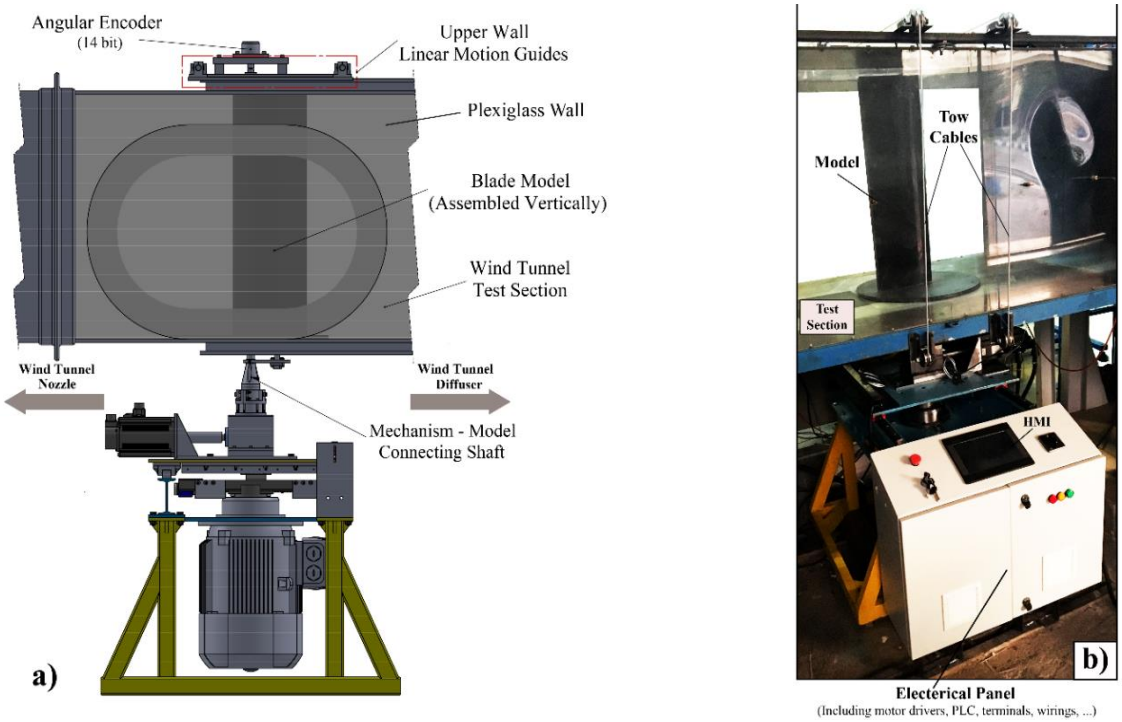

Fig. 2. a) Schematic of integration arrangement of blade motion oscillator and wind tunnel test section, b) Installation of model on motion oscillator integrated with a wind tunnel test section

3. Results and Discussion

The behaviour and aerodynamic loads of a section of a wind turbine were studied in this investigation that two oscillating motions were blade undergoing: pure pitch and pure plunge. As

specified below Oscillations were performed from low to high angles of attack, in the same reduced frequency, in the vicinity and beyond the static stall angles of attack of this airfoil. At a constant Reynolds number of 0.27×10^6, static and dynamic data were acquired. For the pure pitch and pure plunge motion, the average angles of attack were set to 6°, 10°, 15° and the amplitude of the plunge motion was set to 62mm. although, the amplitude of pitch oscillation was set to 2°. The reduced frequency was set to k=0.06 in both motions. In the plunge oscillation, by the following equation, the equivalent angle of attack can be calculated.

$$\alpha_{plunge} = \tan^{-1}\left(\frac{\dot{h}}{U_\infty}\right) \cong \frac{\dot{h}}{U_\infty} \quad \text{For small angles of attack} \tag{1}$$

The angle of attack, oscillation amplitude, reduced frequency, and Reynolds number were almost equal for both pitch and plunge oscillations. For a better comparison of the results and the corresponding differences between the pitch and plunge aerodynamic data, the pressure distribution was studied as a function of angle of attack in three different regions, namely prior to, vicinity to, and beyond the static stall at specific pressure ports on the upper and lower surfaces of the airfoil. Given their importance in airfoil design, the points at x/c=0 (the leading-edge), x/c=0.15, x/c=0.5, x/c=0.8, and x/c=1 (the trailing-edge) were considered. The behaviour of the aerodynamic load during the pitch and plunge oscillations is then compared under almost identical conditions by integrating the pressure coefficients.

Figure 3 compares variations of the measured lift coefficient data with angles of attack with those obtained by CFD and Xfoil [20] codes for a constant Reynolds number of 0.27×10^6. Note that the experimental lift data is obtained through integrating the measured surface pressure at each angle of attack. The numerical modelling, a Lagrangian- Euler pressure-based algorithm is used on an unstructured grids using a K-ωSST turbulence model [21]. A total of 4×10^5 grid were used and the residual convergence order was set to10^{-6}. As seen clearly, the experimentally measured stall angle ranges from 11° to 12°, which is in good agreement with the numerical predictions. There is a slight difference between the experimental and numerical results prior to the static stall angle which is attributed to various errors involved in the numerical modelling [7].

Table 1 and 2 show the test plan for both pure pitch and plunge motions at three different maximum angles of attack cases of prior, vicinity and before the static stall. All data are obtained at a constant Reynolds number of $Re=0.27\times10^6$ and constant reduced frequency k=0.06.

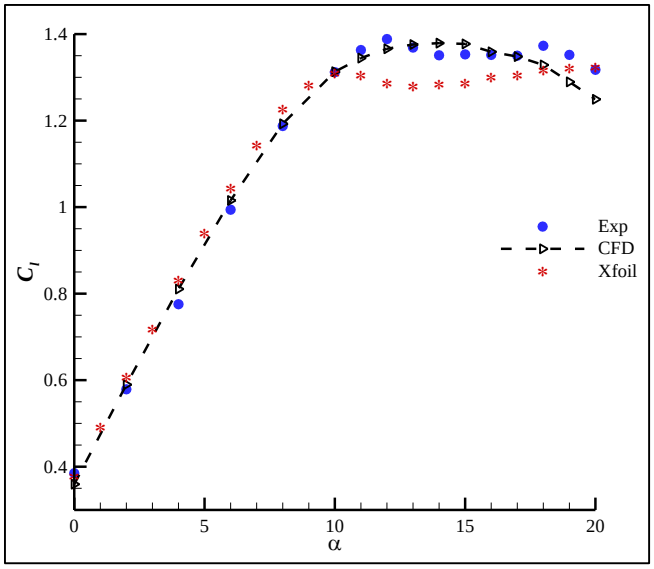

Fig. 3. Variation of C_l vs. α for the static tests

Table 1
Test plan of pitch motion

Pitch motion	
Re=0.27×10^6	
K=0.06	
α_{mean}°	dα°
6°	
10°	2°
15°	

Table 2
Test plan of plunge motion

Plunge motion	
Re=0.27×10^6	
K=0.06	
α_{mean}°	dh(mm)
6°	
10°	62
15°	

3.1 Pressure Distribution

Figure 4 to Figure 6 illustrate the variations of pressure coefficients with the angle of attack for the upper and lower airfoil surfaces. Note that the equivalent angle of attack used for the plunge motion is about 2°, in fact, the equivalent angle of attack obtained from Eq. (1).

When $\alpha < \alpha_{\text{static stall}}$, Figure 4 shows variations of pressure coefficient for the pitch and plunge motions under different pressure conditions over the upper and lower surfaces of the airfoil. Due to the lag of the pressure on the model surface during upstroke and down stroke, pressure hysteresis loops are formed over the upper and lower surfaces and this loops will have counter clockwise direction on the lower surface. As illustrated in Figure 4, for both motions, the width of pressure hysteresis loop and its slope are reduced by moving from the leading edge to the trailing edge. This reduction in width, is more evident in a plunge motion. In both motions, the hysteresis loop is the widest at the leading edge. The hysteresis loop formed over the upper surface under identical

pressure conditions is wider in the plunge motion compared to that of the pitch motion. At the pressure ports at the end of an airfoil, C_p exhibits small variations with the angle of attack, and $|C_p|$ remaining marginally close in the two motions during both upstroke and down stroke, which indicates that pressure variations at the end of an airfoil subject to favourite pressure gradient are not significantly affected by the oscillation type (i.e., pitch or plunge). Additionally, the variations in the pitch motion were observed to be considerably smaller than those in the plunge motion.

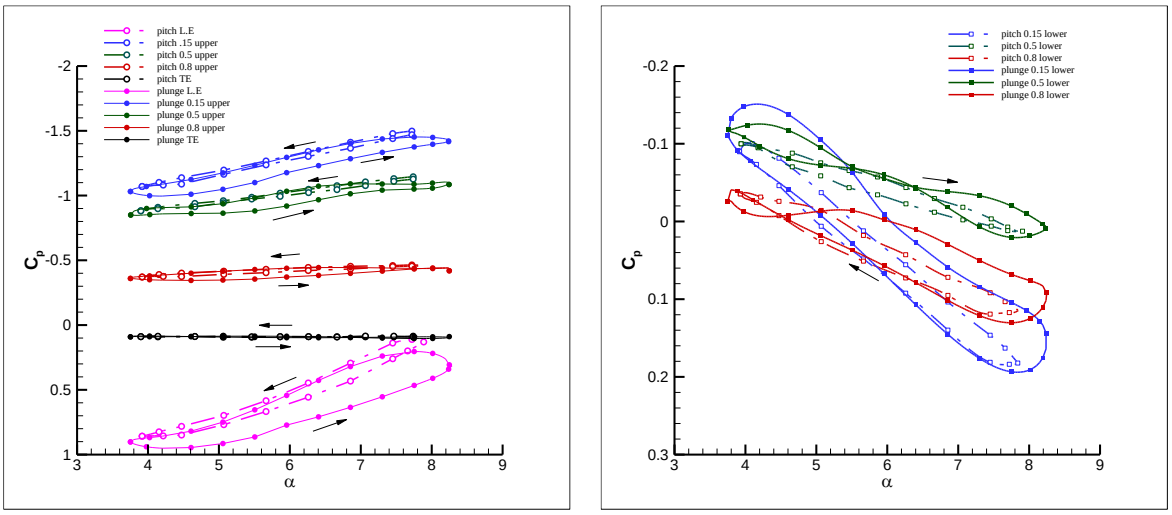

(a) upper (b) lower

Fig. 4. Variation of C_p vs. angle of attack, $\alpha < \alpha_{\text{static-stall}}$

Figure 5 illustrates pressure variations under different conditions near the static stall region. The hysteresis loops assume a counter clockwise direction over the upper surface. As evident, the pressure hysteresis loop is wider in a plunge motion than that in a pitch motion at pressure ports in areas with a favourite pressure gradient. The hysteresis loop assumes a clockwise direction at pressure ports located on the lower surface of the airfoil in both pitch and plunge motions. The effect of the pressure gradient is similar for both pitch and plunge motions. In this region, at the leading edge, $|C_p|$ is higher in the pitch motion than in the plunge motion. However, this difference becomes smaller closer to the trailing edge, where the difference is minimized during upstroke and down stroke, practically levelling out the line.

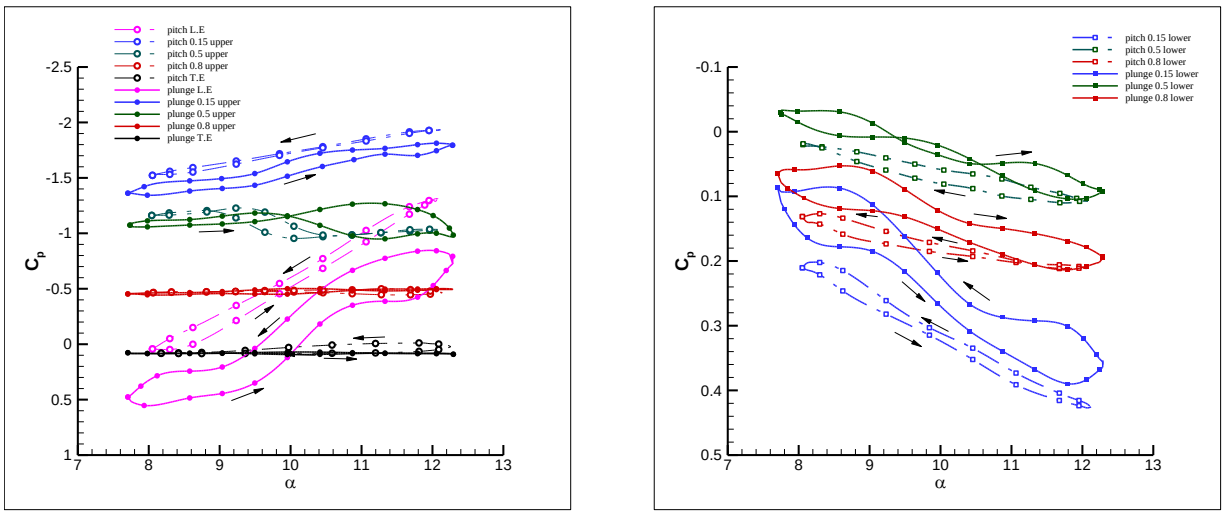

(a) upper (b) lower

Fig. 5. Variation of C_p vs. angle of attack, $\alpha \approx \alpha_{\text{static stall}}$

Figure 6 shows the variations of pressure coefficient over the airfoil surface after the static stall region as the mean angle of attack increases. As shown, the highest suction occurs at the leading edge, in which case the maximum dynamic $|C_p|$ occurs at the maximum angle of attack, the slope of the pressure hysteresis loop is relatively high, and the $|C_p|$ is higher in the plunge motion than in the pitch motion. As shown in Figure 3, the static stall occurs at 11–12° angles of attack. When the model oscillates at $\alpha > \alpha_{static\ stall}$, it is possible to generate a dynamic stall. Two phenomena contribute to the formation of dynamic stall: 1) effect of time-lag of pressure gradient on the development of the boundary layer, and 2) the leading-edge effect. During the upstroke of the leading edge of the airfoil, a behaviour similar to the motion of two side-by-side jets is exhibited by the boundary layer between the stagnation and separation points which can be modelled using the rotational motion of a cylinder. This boundary layer assumes a fuller profile compared to the static cases and delays the separation phenomenon. During down stroke, however, the result is reversed, and the conditions change in favour of separation. At the trailing edge pressure port, the pressure loop is wider in the plunge motion than in the pitch motion and, unlike the previous two regions, pressure variations are not constant. Figure 6(b) shows that pressure coefficient variations at the lower airfoil surface. As shown, the pressure hysteresis loop in this region, similar to that of the upper surface, assumes a clockwise direction. As demonstrated by Figures 6(a) and 6(b), beyond the static stall region, the variations of dynamic pressure at the pressure ports located at the end of the airfoil i.e., x/c=1 and x/c=0.85 are significant compared to the areas before and near static stall, indicating the effect of oscillation on pressure variations in these regions. Note that the effect is more pronounced in the plunge motion.

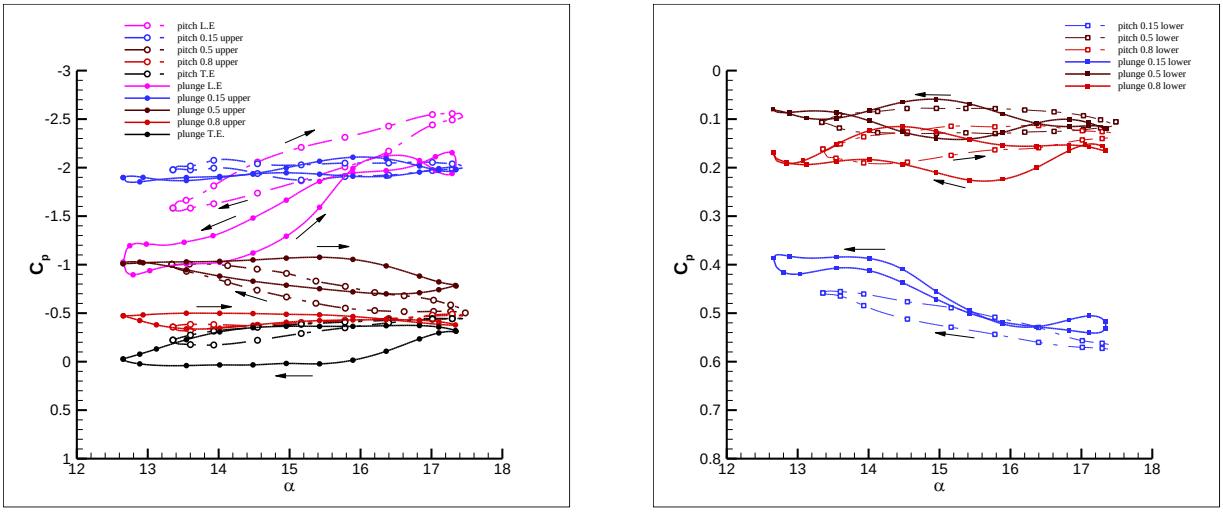

(a) upper (b) lower

Fig. 6. Variation of C_p vs. angle of attack, $\alpha > \alpha_{static\ stall}$

3.2 Aerodynamic Forces

Figure 7 illustrates C_L variations with the angle of attack in the before static stall region. A comparison of the lift hysteresis loop for the pitch and plunge oscillations in the before stall region reveals the loop width to be narrower in the pitch motion than in the plunge motion, suggesting a longer time-lag in the plunge motion at a same reduced frequency and mean angle of attack than in the pitch motion. As the angle of attack increases, the flow-field senses the delayed motion of the model, causing a delay in the lift in upstroke part of motions. The hysteresis loops are counter clockwise in both motions, and the amount of lift during down stroke part of motion is higher than that of the upstroke.

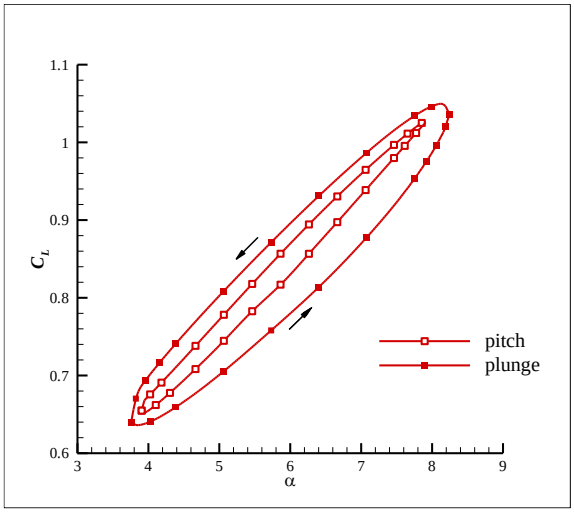

Fig. 7. Variation of C_L vs. angle of attack for $\alpha_{max} < \alpha_{static\text{-}stall}$

Figure 8 shows variation of the lift coefficient with angle of attack in the vicinity of the static stall for both pitch and plunge motions. As depicted in Figure 8, by increasing the angle of attack, the hysteresis loop assumes an 8-shaped form in the pitch motion near static stall region and about an angle of 9.5°, where the hysteresis loop experiences a phase change from lag to lead. Considering the oscillation range, the 8-shaped phenomenon can be attributed to the flow separation on the surface, which flow reattaches due to down stroke part of the motion. In this region, the counter clockwise hysteresis loop is still wider in the plunge motion than that in the pitch motion. Nevertheless, contrary to the pre-stall region, the lift during the upstroke and down stroke courses of the plunge motion is lower than that in the pitch motion.

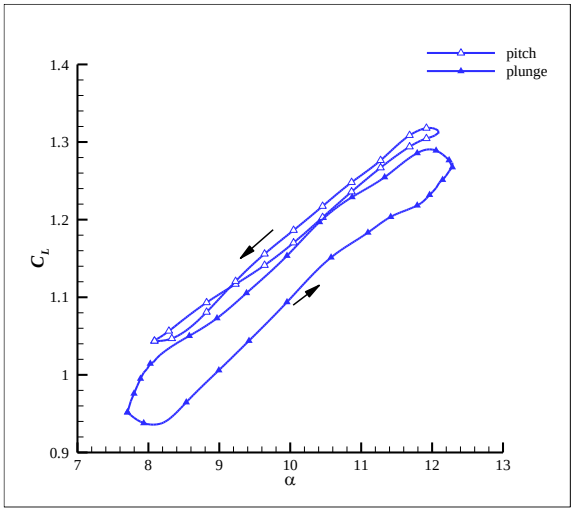

Fig. 8. Variation of C_L vs. angle of attack for $\alpha_{max} \approx \alpha_{static\text{-}stall}$

Figure 9 shows the lift coefficient variations in the beyond static stall region. As evident, the hysteresis loop rotates clockwise. The change in the rotation direction can be associated with the time-lag effect and formation of vortices behind the airfoil. The direction of the hysteresis loop when the model oscillates at low angles of attack is strongly dependent on the leading-edge wake and apparent mass. As the angle of attack increases and causes the model to oscillate near and after the static stall region, an extensive separation region forms on the airfoil and the dynamic stall vortices

play a significant role in the behaviour of the hysteresis loop. By comparing the hysteresis loop in the pitch and plunge motions, two cross over loops are found in the plunge motion, steadily switching from C.W to C.C.W and vice versa. Formation of the two 8-shaped loops can be explained by the separation and reattachment of the flow field that occurred on the suction surface of the airfoil. The hysteresis loop (α=15°) is wider in this case than the two previous ones (α=10°, 6°) and in the pitch motion than the plunge motion. Moreover, the maximum lift coefficient in the plunge motion is larger than that of the pitch motion. In this region, the slope of the hysteresis loop is greater in the plunge motion compared to the pitch motion.

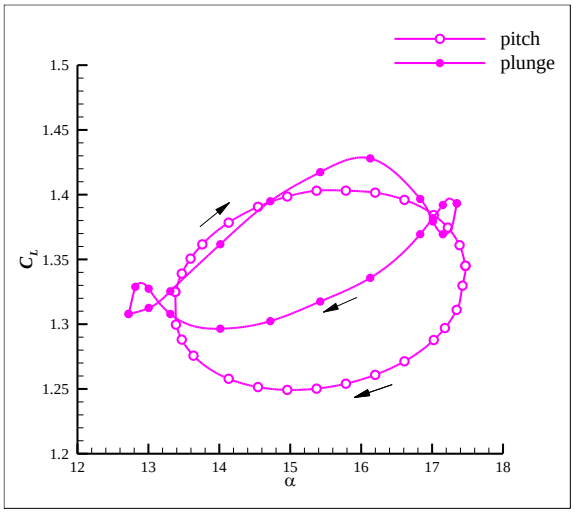

Fig. 9. Variation of C_L vs. angle of attack for $\alpha_{max} > \alpha_{static-stall}$

Differences of the lift coefficient at three regions: prior, vicinity and beyond the static stall angle of attack were shown in Table 3.

Table 3
Differences of lift coefficient in two motions of pitching and plunging at three mean angles of attack

Operational region of the model	α_{mean}	Pure pitch		Pure plunge	
		K=0.06			
		Upstroke	Downstroke	Upstroke	Downstroke
Prior to the static stall angle of attack	6°	0.83	0.87	0.9	0.77
Near the static stall angle of attack	10°	1.16	1.18	1.09	1.15
Beyond the static stall angle of attack	15°	1.39	1.24	1.4	1.3

Figure 10 demonstrates variations of moment coefficient around C/4 with the angle of attack in the pre-static stall region. The clockwise direction of the hysteresis loop in the pitch motion indicates negative aerodynamic damping and instability during the oscillations. The 8-shaped hysteresis loop in the plunge motion causes the direction of the diagram to change from clockwise to counter clockwise. Larger positive moments are observed in the plunge motion as compared to the pitch motion, except for angles of attacks at the end of upstroke in both pitch and plunge motions.

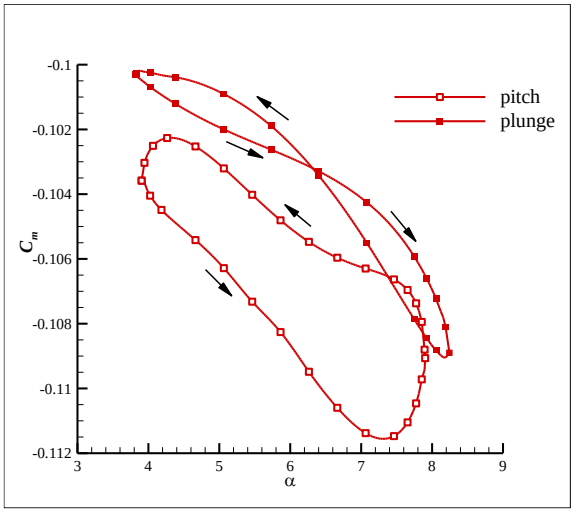

Fig. 10. Variation of C_m vs. angle of attack for $\alpha_{max} < \alpha_{static\text{-}stall}$

As the angle of attack increases, the hysteresis loop near the static stall region in both pitch and plunge motions assumes a counter clockwise direction, indicating positive, stable aerodynamic damping under both types of oscillations. Nevertheless, the moment hysteresis loop has practically the same width in both motions (Figure 11).

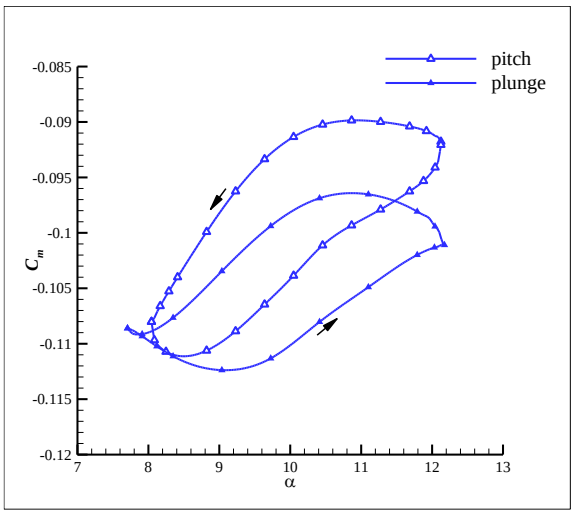

Fig. 11. Variation of C_m vs. angle of attack for $\alpha_{max} \approx \alpha_{static\text{-}stall}$

Figure 12 shows a clockwise hysteresis loop for both pitch and plunge motions in this region so that the hysteresis loop of the pitching moment coefficient is located higher than that of the plunge motion. The moment coefficient of the upstroke and down stroke pitch motion is greater than that in the plunge motion.

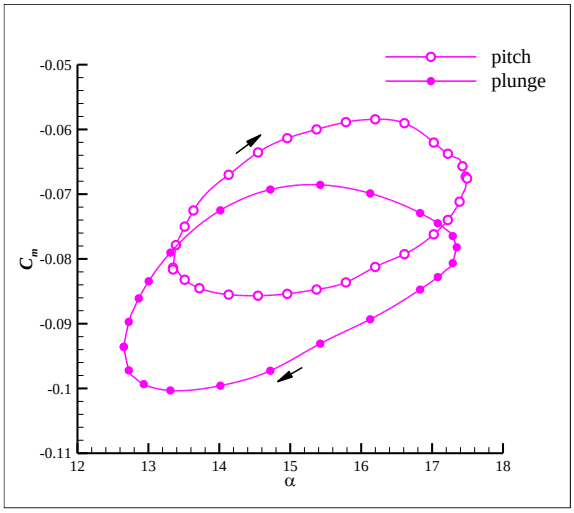

Fig. 12. Variation of C_m vs. angle of attack for $\alpha_{max} > \alpha_{static\text{-}stall}$

4. Conclusions

During the operation of wind turbine blade, it is experiences to pitch or plunge oscillations together or separately. Therefore, identification of the physics of pitch and plunge oscillations in the same conditions such as the amplitude of oscillation and reduced frequency, also helps to better understand the fluid physics around the wind turbine blade. This can be used to improve the aerodynamic performance of wind turbine blade. As improve the aerodynamic performance of wind turbine blade, wind turbine production power is increased.

Extensive experimental studies have been conducted to investigate the aerodynamic behaviour of wind turbine blade cross-sections under oscillatory motions. The aerodynamic forces acting on a model can be calculated by measuring the pressure distribution over the upper and lower surfaces of the model while changing the effective parameters such as the initial angle of attack, reduced frequency, oscillations amplitude and Reynolds number. In this study, pure plunge and pitch motions were investigated under same oscillatory conditions by setting identical values for the initial angle of attack, reduced frequency and amplitude of oscillation in both motions. The model was separately subjected to pitch and plunge motions at a fixed Reynolds number of 0.27×10^6, and the aerodynamic loads induced by oscillations were investigated by measuring the pressure distribution. The main results are summarized as follows

i. In the region before the static stall angles of attack, the hysteresis loop of the lift coefficient in the pitch motion is inserted into that of the plunge motion. At the same angle of attack in both upstroke and down stroke cases, the generated lift force in the pitch motion was greater than that in the plunge motion.
ii. As the mean angle of attack increased in the region near the static stall angle of attack, the thickness of the hysteresis loop of the lift coefficient was reduced in both pitch and plunge motions, while the width of the hysteresis loop in the plunge motion was greater than that in the pitch motion. Nevertheless, the generated lift in both down stroke and upstroke cases during the pitch motion was greater than that of the plunge motion. Hence, when a greater lift is required in practice, the model should be subjected to pitch motion in the region near the static stall rather than before the static stall.
iii. With increasing the angle of attack beyond the static stall, the width of the hysteresis loop for the lift coefficient was increased due to the delay caused by flow separation and reattach in

both pitch and plunge motions. Unlike the regions before and near the static stall, the upstroke lift coefficient in this region was greater than down stroke lift coefficient in both pitch and plunge oscillations. An insignificant difference was observed between the upstroke lift coefficients in the pitch and plunge motions in the beginning of the region after the static stall. However, this difference was increased as the angle of attack increased by moving away from the vicinity of the static stall.

iv. In the region beyond the static stall angles of attack, the slope of the hysteresis loop for the lift coefficient was smaller in the pitch motion than that in the plunge motion. As a result, the plunge motion generated a greater lift compared to the pitch motion after the static stall.

v. The width of the hysteresis loop of the pitching moment was increased by increasing the mean angle of attack in both motions. In the region before the static stall, the hysteresis loop of the pitching moment in the plunge motion was located entirely above that in the pitch motion. At a given angle of attack in this region, the plunge motion generated a more positive pitching moment compared to the pitch motion.

References

[1] Rasti, Ehsan, Farhad Talebi, and Kiumars Mazaheri. "A turbulent duct flow investigation of drag-reducing viscoelastic FENE-P fluids based on different low-Reynolds-number models." *Physica A: Statistical Mechanics and its Applications* 526 (2019): 120718.

[2] Souza, Paulo Victor Santos, and Daniel Girardi. "Drag force in wind tunnels: A new method." *Physica A: Statistical Mechanics and its Applications* 467 (2017): 120-128.

[3] Paiva, Aureliano Sancho Souza, Miguel Angel Rivera-Castro, and Roberto Fernandes Silva Andrade. "DCCA analysis of renewable and conventional energy prices." *Physica A: Statistical Mechanics and its Applications* 490 (2018): 1408-1414.

[4] Stef Stefanello, M. B., G. A. Degrazia, L. Mortarini, L. Buligon, S. Maldaner, J. C. Carvalho, O. C. Acevedo et al. "Development of an analytical Lagrangian model for passive scalar dispersion in low-wind speed meandering conditions." *Physica A: Statistical Mechanics and its Applications* 492 (2018): 1007-1015.

[5] Puhales, Franciano Scremin, Giuliano Demarco, Luis Gustavo Nogueira Martins, Otávio Costa Acevedo, Gervásio Annes Degrazia, Guilherme Sausen Welter, Felipe Denardin Costa, Gilberto Fernando Fisch, and Ana Cristina Avelar. "Estimates of turbulent kinetic energy dissipation rate for a stratified flow in a wind tunnel." *Physica A: Statistical Mechanics and its Applications* 431 (2015): 175-187.

[6] Shi, Feng, and Ning Huang. "Measurement and simulation of sand saltation movement under fluctuating wind in a natural field environment." *Physica A: Statistical Mechanics and its Applications* 391, no. 3 (2012): 474-484.

[7] Hassan, Gasser Elhussien, Amany Hassan, and Mohamed Elsayed Youssef. "Numerical investigation of medium range re numbers aerodynamics characteristics for naca0018 airfoil." *CFD letters* 6, no. 4 (2015): 175-187.

[8] Hamizi, Ilya Bashiera, and Sher Afghan Khan. "Aerodynamics Investigation of Delta Wing at Low Reynold's Number." *CFD Letters* 11, no. 2 (2019): 32-41.

[9] Dehkordi, Mohammad Hossein Razavi, Mohammad Reza Soltani, and Ali Reza Davari. "Statistical analysis on the effect of reduced frequency on the aerodynamic behavior of an airfoil in dynamic physical motions." *Physica A: Statistical Mechanics and its Applications* 535 (2019): 122450.

[10] Soltani, Mohammad Reza and Rasi Marzabadi, Faezeh. "Effect of Reduced Frequency on the Aerodynamic Behavior of an Airfoil Oscillating in a Plunging Motion." *Scientia Iranica* 16, no. 1 (2009): 40-52.

[11] Kim, Dong-Ha, and Jo-Won Chang. "Low-Reynolds-number effect on the aerodynamic characteristics of a pitching NACA0012 airfoil." *Aerospace Science and Technology* 32, no. 1 (2014): 162-168.

[12] Guo, Yonghui, Xiaochang Li, Lanxin Sun, Ye Gao, Zheming Gao, and Linjun Chen. "Aerodynamic analysis of a step adjustment method for blade pitch of a VAWT." *Journal of Wind Engineering and Industrial Aerodynamics* 188 (2019): 90-101.

[13] Ansari, M., M. R. H. Nobari, and E. Amani. "Determination of pitch angles and wind speeds ranges to improve wind turbine performance when using blade tip plates." *Renewable Energy* 140 (2019): 957-969.

[14] Moriche, Manuel, Oscar Flores, and Manuel García-Villalba. "On the aerodynamic forces on heaving and pitching airfoils at low Reynolds number." *Journal of Fluid Mechanics* 828 (2017): 395-423.

[15] Tabrizian, A., M. Masdarf, and M. Tahani. "Surface Pressure Study of am Airfoil Undergoing Combined Pitch and Low-Amplitude Plunge Motions." *Journal of Applied Fluid Mechanics* 12, no. 6 (2019):1957-1966.

[16] Gross, A., M. Agate, J. Little, and Hermann F. Fasel. "Numerical Simulation of Plunging Wing Section at High Angles of Attack." *AIAA Journal* 56, no. 7 (2018): 2514-2527.
[17] Geng, F., I. Kalkman, A. S. J. Suiker, and B. Blocken. "Sensitivity analysis of airfoil aerodynamics during pitching motion at a Reynolds number of 1.35× 105." *Journal of Wind Engineering and Industrial Aerodynamics* 183 (2018): 315-332.
[18] Kunya, Bashir Isyaku, Clement O. Folayan, Gyang Yakubu Pam, Fatai Olukayode Anafi, and Nura Muaz Muhammad. "Experimental and Numerical Study of the Effect of Varying Sinusoidal Bumps Height at the Leading Edge of the NASA LS (1)-0413 Airfoil at Low Reynolds Number." *CFD Letters* 11, no. 3 (2019): 129-144.
[19] Leknys, R. R., M. Arjomandi, R. M. Kelso, and C. H. Birzer. "Leading-edge vortex development on a pitching flat plate with multiple leading edge geometries." *Experimental Thermal and Fluid Science* 96 (2018): 406-418.
[20] Drela, Mark. "XFOIL: An analysis and design system for low Reynolds number airfoils." In *Low Reynolds number aerodynamics*, pp. 1-12. Springer, Berlin, Heidelberg, 1989.
[21] Menter, Florian R. "Two-equation eddy-viscosity turbulence models for engineering applications." *AIAA journal* 32, no. 8 (1994): 1598-1605.